Exploring the Tropically Excited Arctic Warming Mechanism with Station Data: Links between Tropical Convection and Arctic Downward Infrared Radiation

MATTHEW D. FLOURNOY AND STEVEN B. FELDSTEIN

Department of Meteorology, The Pennsylvania State University, University Park, Pennsylvania

SUKYOUNG LEE

Department of Meteorology, The Pennsylvania State University, University Park, Pennsylvania, and School of Earth and Environmental Sciences, Seoul National University, Seoul, South Korea

EUGENE E. CLOTHIAUX

Department of Meteorology, The Pennsylvania State University, University Park, Pennsylvania

(Manuscript received 23 September 2014, in final form 19 August 2015)

ABSTRACT

The Tropically Excited Arctic Warming (TEAM) mechanism ascribes warming of the Arctic surface to tropical convection, which excites poleward-propagating Rossby wave trains that transport water vapor and heat into the Arctic. A crucial component of the TEAM mechanism is the increase in downward infrared radiation (IR) that precedes the Arctic warming. Previous studies have examined the downward IR associated with the TEAM mechanism using reanalysis data. To corroborate previous findings, this study examines the linkage between tropical convection, Rossby wave trains, and downward IR with Baseline Surface Radiation Network (BSRN) downward IR station data. The physical processes that drive changes in the downward IR are also investigated by regressing 300-hPa geopotential height, outgoing longwave radiation, water vapor flux, ERA-Interim downward IR, and other key variables against the BSRN downward IR at Barrow, Alaska, and Ny-Ålesund, Spitsbergen.

Both the Barrow and the Ny-Ålesund station downward IR anomalies are preceded by anomalous tropical convection and poleward-propagating Rossby wave trains. The wave train associated with Barrow resembles the Pacific–North America teleconnection pattern, and that for Ny-Ålesund corresponds to a northwestern Atlantic wave train. It is found that both wave trains promote warm and moist advection from the midlatitudes into the Arctic. The resulting water vapor flux convergence, multiplied by the latent heat of vaporization, closely resembles the regressed ERA-Interim downward IR. These results suggest that the combination of warm advection, latent heat release, and increased cloudiness all contribute toward an increase in downward IR.

1. Introduction

According to the Tropically Excited Arctic Warming (TEAM) mechanism, proposed by Lee et al. (2011) and Lee (2012), La Niña–like convection over the tropical Pacific excites poleward-propagating Rossby waves that warm the Arctic via an intensified poleward eddy heat flux, eddy-induced adiabatic descent, and an increase in downward infrared radiation (IR). These wave trains take about 10 days to propagate from the tropics to high latitudes (Hoskins and Karoly 1981). Thus, the TEAM mechanism is fundamentally an intraseasonal-time-scale process. The TEAM mechanism has been shown to operate on the intraseasonal time scale in connection with the tropical Madden–Julian oscillation (MJO) (Yoo et al. 2011, 2012a,b), on the interannual time scale in association with the El Niño–Southern Oscillation

Corresponding author address: Steven Feldstein, Department of Meteorology, The Pennsylvania State University, 503 Walker Building, University Park, PA 16802.
E-mail: sbf1@meteo.psu.edu

DOI: 10.1175/JAS-D-14-0271.1

(Lee 2012), and on the interdecadal time scale (Lee et al. 2011), possibly linked to greenhouse gas warming.

In previous studies, the downward IR associated with the TEAM mechanism was examined with ERA-40 and ERA-Interim data. As the reanalysis IR data are model generated, to corroborate the key role played by downward IR for the TEAM mechanism, we examine whether tropical convection and poleward-propagating Rossby wave trains are associated with changes in downward IR at various surface stations in the Arctic. For this purpose, we use daily downward IR data from the following two World Radiation Monitoring Center–Baseline Surface Radiation Network (BSRN) stations: Barrow, Alaska (71°N, 156°W), and Ny-Ålesund, Spitsbergen (78°N, 11°E) (Dutton et al. 2014; Maturilli et al. 2014).

In the recent modeling study of Yoo et al. (2012a), it was found that the tropically excited wave train transports a passive tracer poleward, alluding to the possibility that increases in downward IR associated with the TEAM mechanism arise from poleward water vapor transport and an attendant increase in downward IR. Motivated by that result, we also examine the relationship between poleward water vapor transport and changes in liquid water and ice content associated with changes in downward IR at the above Arctic stations. As we will see, a strengthened poleward water vapor transport occurs in conjunction with increased water vapor flux convergence, condensation, latent heat release, increased cloudiness, warm advection, and a greater downward IR. Because of the close relationship between reanalysis and station downward IR, these findings suggest that a similar process may drive an increase in downward IR and surface warming over much of the Arctic.

In section 2, the data and methods are presented, followed by the results in section 3 and the summary and conclusions in section 4.

2. Data and methods

As discussed in the introduction, the downward IR data used in this study consist of time series from two BSRN stations. The downward IR measurements were taken by a pyrgeometer at each location and then accumulated forward in time from 0000 UTC to the end of a model time step. For this study, we used the accumulated downward IR data at 0300 UTC, and converted these data to watts per square meter by dividing each value by the 3-h time step. Our analysis uses the daily BSRN downward IR data for the December–February (DJF) winter period spanning 17 winter seasons (1534 days) for both sites. Downward IR data at Alert and Eureka, Canada, and Tiksi, Russia, the remaining BSRN sites in the Arctic, are also available for seven, four, and two DJF seasons, respectively, but their time series are too short to extract conclusions relevant to the focus of this paper.

Our motivation for using daily downward IR data is based on the value of the *e*-folding time scale of the downward IR time series. Figure 1 shows the lagged autocorrelations of the BSRN downward IR at Barrow and Ny-Ålesund. These autocorrelations are calculated separately for each DJF season and then time averaged. As can be seen, for Barrow and Ny-Ålesund, the downward IR time series have *e*-folding time scales of 5 and 3 days, respectively. Since our focus is to investigate the processes that drive anomalies in Arctic downward IR, we use daily downward IR data for this study, rather than data that have been averaged over a much longer time period.

In this study, we perform lagged regressions of the following variables against the daily downward IR time series at the above stations: 300-hPa geopotential height, 2-m temperature, 400-hPa temperature, vertically integrated water vapor flux and its convergence, cloud liquid and frozen water, cloud fraction, and outgoing longwave radiation (OLR). Each regression spans the same time period as the BSRN downward IR time series (i.e., 1993–2010 for Barrow and Ny-Ålesund). For each of these calculations, except those with OLR data, we use European Centre for Medium-Range Weather Forecasts (ECMWF) ERA-Interim data (Dee and Uppala 2009; Dee et al. 2011); several recent studies showed that the ERA-Interim dataset is the most reliable one in representing Arctic climate. The OLR data are obtained from the National Oceanic and Atmospheric Administration (NOAA) and are used as a proxy for deep convection in the tropics. We also regress the daily, multivariate MJO index of Wheeler and Hendon (2004) against the downward IR time series. The MJO index is defined as the principal component time series of the two leading combined EOFs of the 200- and 850-hPa zonal wind and the OLR, latitudinally averaged from 15°S to 15°N. With the exception of the MJO index, all fields are represented on a global 2.5° latitude by 2.5° longitude grid.

For the lagged regressions, we specify a one-standard-deviation anomaly for the downward IR time series. Statistical significance is determined from the Pearson correlation *r*, with the number of degrees of freedom (NDOF) estimated using the procedure of Davis (1976): that is,

$$\mathrm{NDOF} = N\delta t/\tau \tag{1}$$

and

$$\tau = \sum_{a} C_x(a)C_y(a)\,\delta t, \tag{2}$$

where N is the number of days for a specific, lagged time series, δt is the time interval between adjacent values

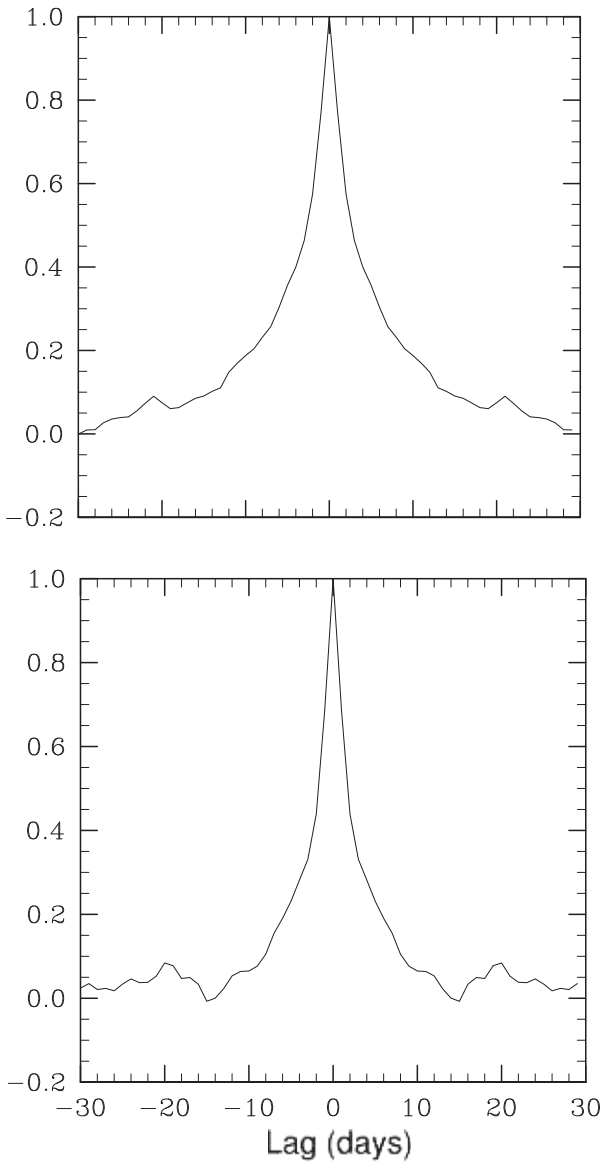

FIG. 1. Lagged autocorrelation functions for the (top) Barrow and (bottom) Ny-Ålesund BSRN downward IR time series. Autocorrelations are calculated separately for each DJF season and then time averaged.

(1 day), and C_x and C_y are lagged autocorrelations of station downward IR and the regressed field, respectively, where a is the lag.

3. Results

a. Barrow downward IR

As indicated in the introduction, an increase in ERA-Interim downward IR over the Arctic Ocean is accompanied by an increase in the Arctic 2-m temperature (Lee et al. 2011; Yoo et al. 2012b). We examine whether a similar relationship occurs with station data by regressing the 2-m temperature field against Barrow's BSRN downward IR (Fig. 2). Consistent with studies that used ERA downward IR, there is a large statistically significant positive temperature anomaly centered over northern Alaska, which attains its maximum value at lag 0 days (Fig. 2). Another important characteristic of the signal is that the time scales over which 2-m temperature increases before lag 0 and decreases after lag 0 are similar to the Barrow downward IR *e*-folding time scale. These results suggest that increased downward IR is an important contributor to the surface warming in northern Alaska.

Is this downward IR, although taken at a single location, linked to convection and the large-scale atmospheric circulation at lower latitudes? To address this question, we first compute the lagged regression between the downward IR at Barrow and the Northern Hemisphere (NH) 300-hPa geopotential height field (see Fig. 3). A wave train is evident at lag −10 days with positive, statistically significant centers over the west-central tropical Pacific and western Canada–Alaska, along with a negative center (not statistically significant) over the northeastern Pacific. Each of these three centers undergoes growth followed by decay, with the peak amplitude occurring at lag −7 days for the west-central tropical Pacific center, lag −3 days for the northeastern Pacific center, and lag 0 days for the western Canada–Alaska center. This timing, along with the northwest–southeast horizontal tilt of the anomalies, indicates that the wave train is propagating northeastward from the tropical Pacific toward western Canada and Alaska. An additional center extending from the southwestern United States to northeastern Canada also experiences growth and decay, reaching its peak at lag +3 days. The temporal evolution of this four-centered wave train resembles that of the onset of the Pacific–North America (PNA) teleconnection pattern (Feldstein 2002). This relationship is also evident in regressions between the Barrow downward IR and PNA index of the NOAA/Climate Prediction Center (see Fig. 4), which show statistically significant, positive values between lags −17 and −5 days.

Consistent with the presence of the PNA-like pattern, which typically occurs in conjunction with convection anomalies over the tropical Indian and western Pacific Oceans (e.g., Moore et al. 2010; Franzke et al. 2011; Yoo et al. 2012a,b), the Barrow downward IR is also found to be linked to tropical convection. The tropical OLR field regressed against the Barrow downward IR reveals a dipole pattern, with centers of opposite sign over the tropical Indian and western Pacific Oceans (see Fig. 5).

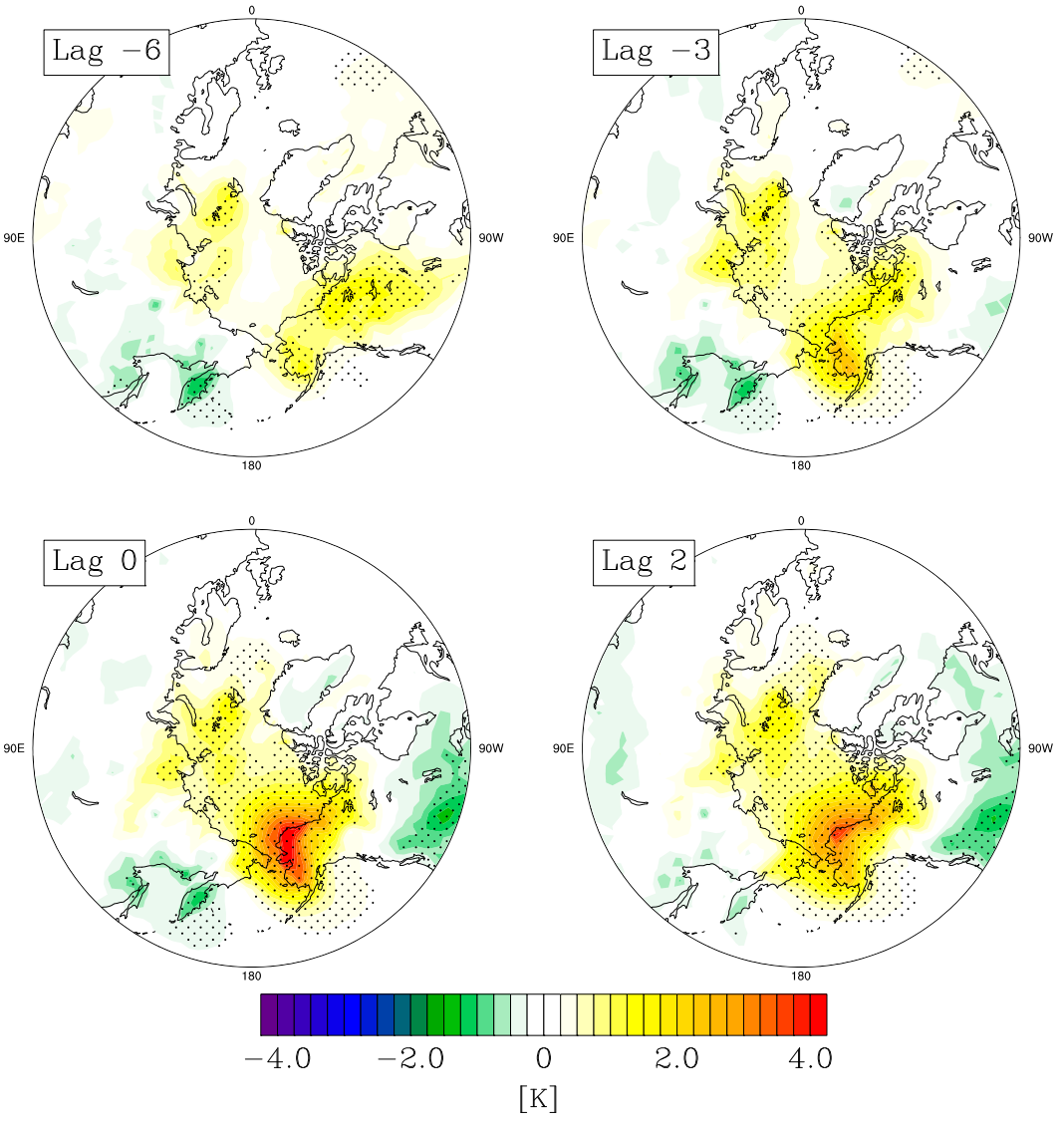

FIG. 2. Lagged regressions of 2-m temperature against the BSRN Barrow downward IR. Dots indicate statistical significance at the 95% confidence level using the method of Davis (1976).

(Note that enhanced convection corresponds to negative OLR anomalies, and vice versa.) During the lag −14 to lag −6 day time period, the Indian Ocean center exhibits steady growth and eastward propagation while the western Pacific Ocean center shows growth and decay with little propagation. The anomaly fields in Figs. 3 and 5 are consistent with the findings of previous studies, which show that increased (decreased) convection over the tropical Pacific Ocean and decreased (increased) convection over the tropical Indian Ocean are followed by the excitation of the positive (negative) PNA pattern. Thus, these results indicate that the station downward IR data at Barrow do indeed have a remote, tropical influence, consistent with previous studies using ERA datasets that link Arctic downward IR to tropical convection via the excitation of poleward-propagating Rossby wave trains.

The spatial characteristics of the 300-hPa geopotential height and OLR anomalies in Figs. 3 and 5 suggest that Barrow downward IR may also be associated with the dominant mode of intraseasonal variability in the tropics, the MJO (e.g., Mori and Watanabe 2008; Johnson and Feldstein 2010; Moore et al. 2010; Roundy et al. 2010; Franzke et al. 2011; Yoo et al. 2012a,b). The features of the MJO can be succinctly illustrated with the multivariate MJO index of Wheeler and Hendon (2004). To examine whether the MJO is related to Barrow downward IR, we regress the two leading

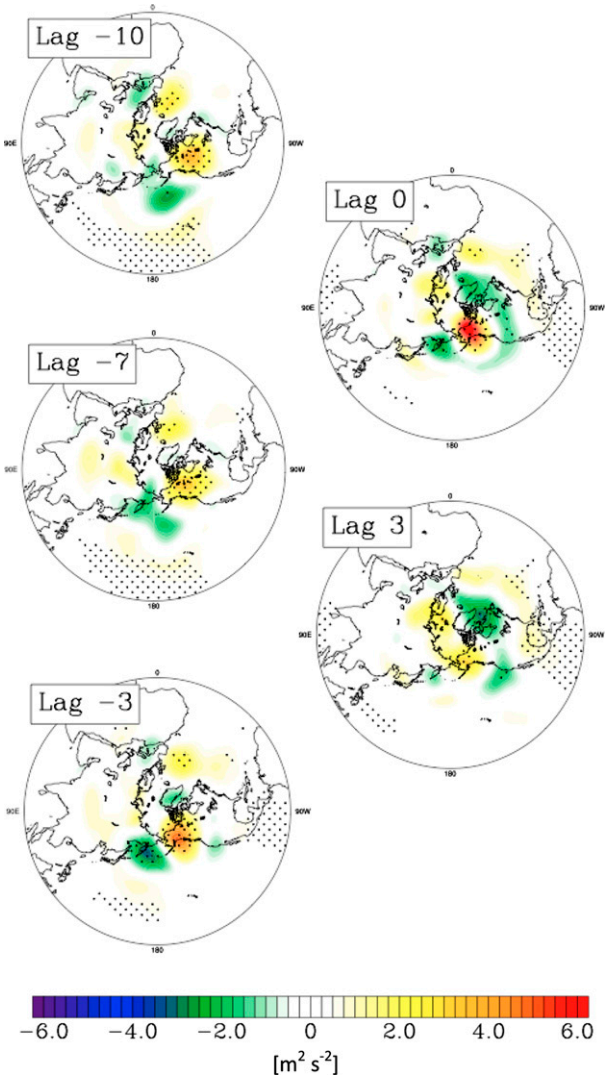

FIG. 3. As in Fig. 2, but for 300-hPa geopotential.

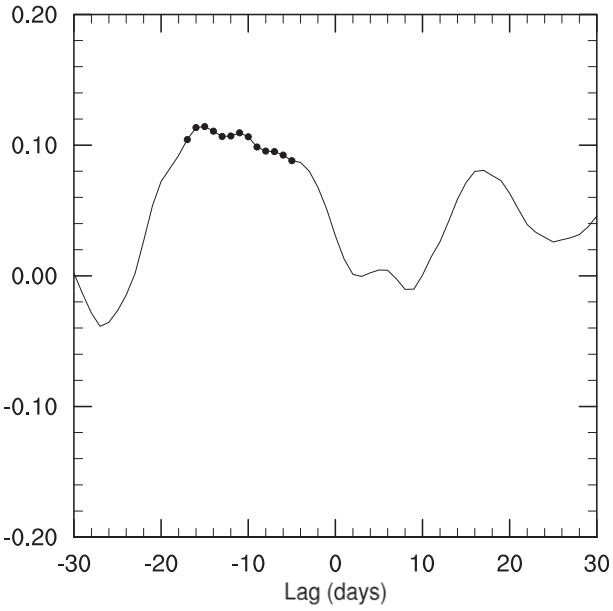

FIG. 4. Lagged regressions of the PNA index against the BSRN Barrow downward IR. Dots indicate statistical significance at the 95% confidence level.

principal component time series—the first and second modes of the real-time multivariate MJO (RMM) index, typically denoted by RMM1 and RMM2—against the Barrow downward IR (Fig. 6). It can be seen that one or both modes is statistically significant at the 95% confidence level every day from lag −18 days to lag +26 days. These regressions indicate eastward propagation of the MJO, with enhanced convection observed over the Maritime Continent at lag −20 days, over the western Pacific by lag −10 days (as shown in Fig. 5), near Africa by lag 0 days, over the Indian Ocean at lag +10 days, and returning to the western Pacific by lag +20 days, thus completing the cycle within about 40 days, a typical period for the MJO. [Figure 8 of Wheeler and Hendon (2004) shows the relationship between the location of increased MJO convection and the values of RMM1 and RMM2.] These findings are chronologically consistent with enhanced tropical convection over the western Pacific Ocean and reduced convection over the Indian Ocean, the excitation of the positive PNA, anomalously strong downward IR episodes at Barrow, and vice versa. This linkage to the MJO further supports the influence of remote tropical convection on downward IR at Barrow.

The above results suggest that the Barrow downward IR anomalies are linked to MJO tropical convection via the Rossby wave train excited by the convection. These results lead to the question of what physical processes account for the relationship between wave train propagation into the Arctic and changes in the Barrow downward IR. One plausible answer involves the advection of water vapor from midlatitudes into northern Alaska by the wave train. Because of the very low saturation vapor pressure over Alaska during the winter, the water vapor advected into Alaska would be expected to readily condense into liquid water and/or ice and lead to increased cloudiness. To examine whether these processes may be taking place, we regress the ERA-Interim vertically integrated water vapor flux and water vapor flux convergence, cloud liquid water and cloud frozen water contents, and downward IR against the Barrow downward IR.

The regressed vertically integrated water vapor flux and water vapor flux convergence are shown in the left column of Fig. 7. (For reasons to be described later, the

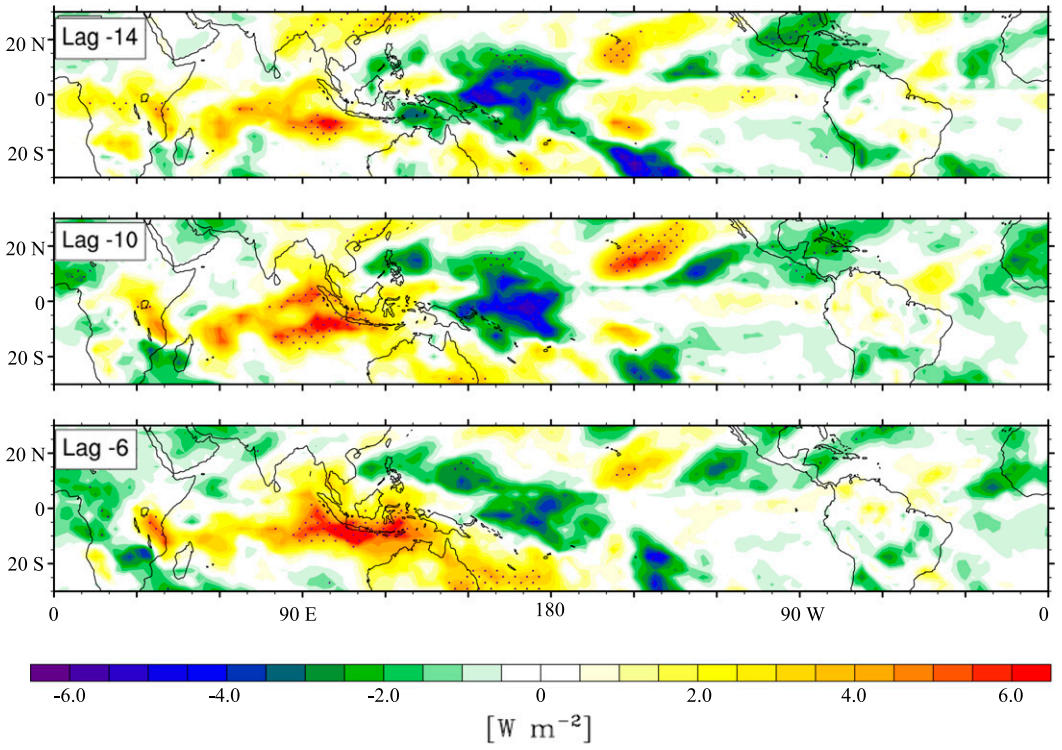

FIG. 5. As in Fig. 2, but for OLR in the tropics.

water vapor flux convergence in Fig. 7 is multiplied by the latent heat of vaporization.) The direction of the water vapor flux vectors shows an anticyclonic circulation centered over the Gulf of Alaska. A very similar circulation is implied by the regressed sea level pressure field (not shown), which suggests that a sizeable contribution to the water vapor flux occurs in the lower troposphere. [Based on potential vorticity dynamics (Hoskins et al. 1985), the Rossby wave train in the upper troposphere (Fig. 3) is expected to induce the sea level pressure anomalies.] As can be seen, water vapor is advected from the midlatitude northeastern Pacific poleward toward Alaska, which results in a region of enhanced water vapor flux convergence that shifts poleward toward Barrow from lag −2 to lag 0 days. Consistently, we see an increase in both cloud liquid water (Fig. 8a) and cloud frozen water (Fig. 8b) by lag 0 days, with the location of the latter being poleward of the former. [Regressions of cloud liquid water flux convergence were also performed (not shown); these regressions were found to be weak and not statistically significant.]

The regressed ERA-Interim downward IR is shown in the center column of Fig. 7. [The regressed downward IR attains its maximum lag-0-day value close to Barrow, which gives us confidence that the ERA-Interim downward IR is similar to that at the BSRN station; this finding is consistent with Zib et al. (2012), who showed with monthly mean data that ERA-Interim downward IR compares reasonably well with the

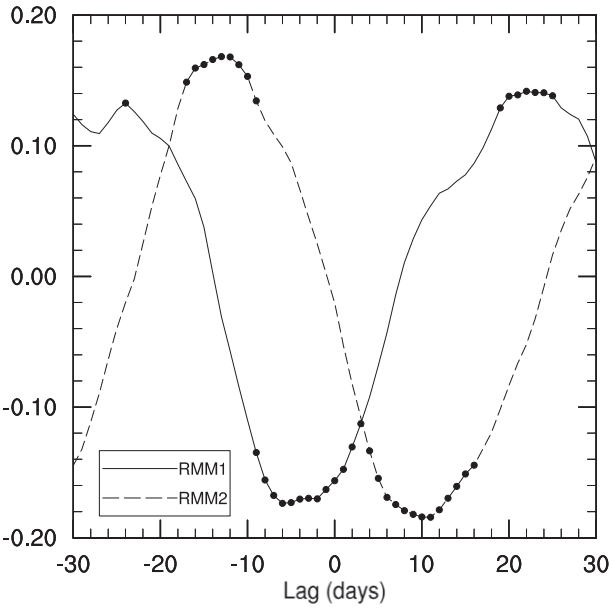

FIG. 6. As in Fig. 4, but for the RMM1 and RMM2 indices.

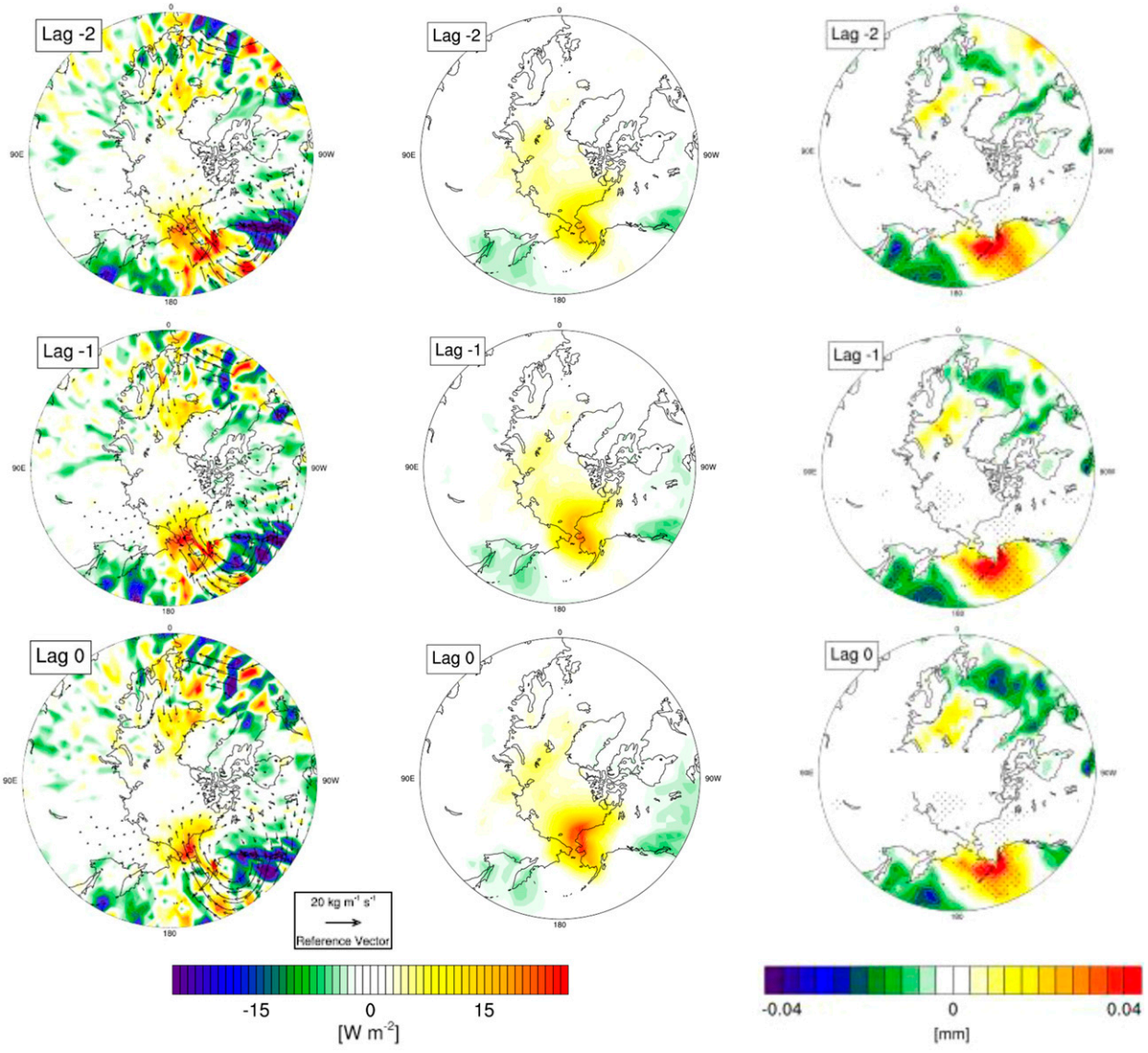

FIG. 7. Lagged regressions of (left) water vapor flux (vectors) and water vapor flux convergence multiplied by the latent heat of vaporization (shading), (center) ERA-Interim downward IR, and (right) surface evaporation against the BSRN Barrow downward IR. Dots indicate statistical significance at the 95% confidence level.

BSRN downward IR at both Barrow and Ny-Ålesund.] As can be seen, the spatial structure and amplitude of the regressed downward IR resemble those of the water vapor flux convergence multiplied by the heat of vaporization. (Since the latent heat of fusion is only about 15% that of the latent heat of vaporization, we simply multiply by the latent heat of vaporization at all locations.) This suggests that the majority of the converged water vapor undergoes condensation with much of the released latent heat being realized in an increased atmospheric temperature and ultimately as an increase in downward IR.

To further examine individual influences on downward IR from a radiative transfer perspective, we calculated cloud cover (cloud fraction) and σT^4 at three different layers in the atmosphere regressed against the Barrow downward IR for lag 0 days, where σ is the Stefan–Boltzmann constant and T is temperature. These layers are defined by the boundaries of the ERA-Interim low, medium, and high cloud layers, which are defined as follows: low clouds, $1.0 > \sigma > 0.8$; medium clouds, $0.8 > \sigma > 0.45$; and high clouds, $\sigma \leq 0.45$. To obtain the σT^4 time series in each of these layers, a layer-averaged T was calculated (using the available

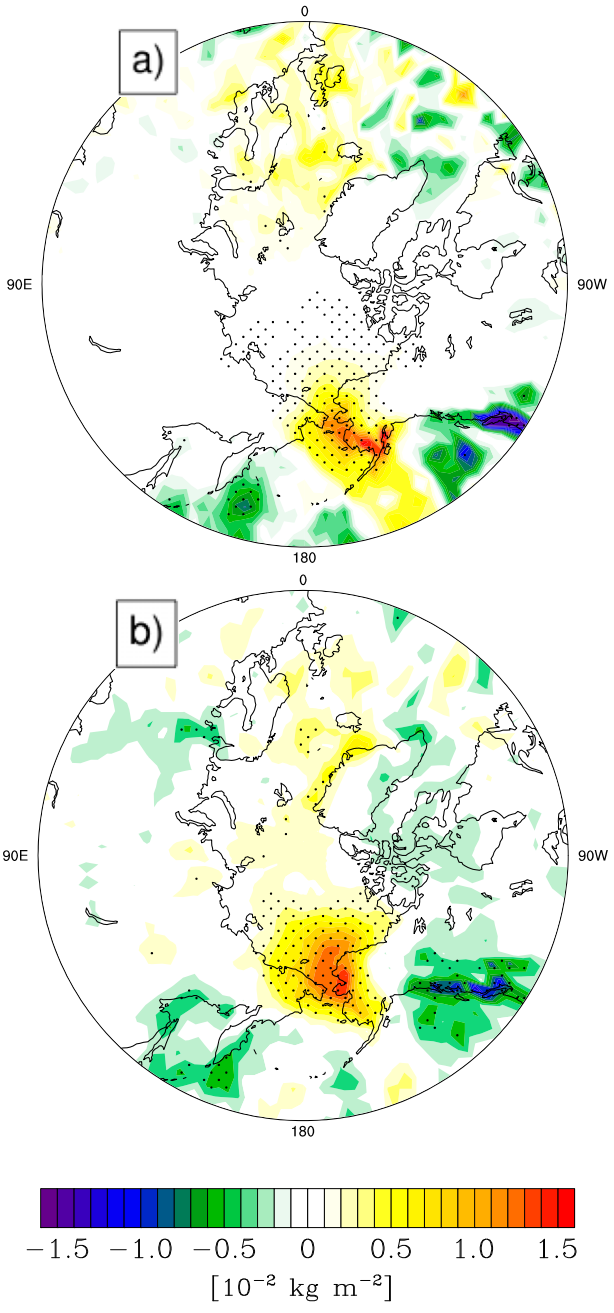

FIG. 8. Lag-0-day regressions of (a) cloud liquid water and (b) cloud frozen water against the BSRN Barrow downward IR. Dots indicate statistical significance at the 95% confidence level.

pressure levels in the ERA-Interim dataset), then raised to the fourth power and multiplied by σ (assuming that the clouds have an emissivity of 1.0).

While a complete, quantitative radiative transfer analysis is beyond the scope of this particular study, much insight can still be gained by examining the cloud cover and σT^4 from the regressions shown below. As can be seen, a one-standard-deviation increase in downward IR is associated with increases in upper and middle layer cloud cover greater than 12% and 8%, respectively (center column, top two panels of Fig. 9). In the lower layer, the connection between Barrow downward IR and cloud cover appears to be dominated by orographic influences associated with the Brooks Range. These mountains are located slightly to the south of Barrow with an east–west orientation. Given the southerly low-level winds associated with the increase in Barrow downward IR, it is likely that the increase in cloudiness to the south of Barrow and subsequent decrease in cloudiness at and to the north of Barrow (a decline of about 5%) (center column, bottom panel of Fig. 9) can be explained by orographic lifting. It is also important to note that the winter-mean cloudiness above Barrow is about 75% in the lower layer and about 30% in the middle and upper layers (right column, Fig. 9). Thus, the lower-layer cloud fraction at Barrow declines to about 70%, and the mid- and upper-layer cloud fractions increase to 38% and 42%, respectively, when the Barrow downward IR increases.

The increase in Barrow downward IR is also associated with a statistically significant warming in all three layers (Fig. 9, left column). It is likely that the warm advection is playing a key role for the warming of all three layers, since the wind field, as implied by the regressed 300-hPa geopotential height (Fig. 3) and the sea level pressure (discussed above), is southerly over Barrow. For the top two layers, because of the increase in cloud fraction, we speculate that this increase in temperature is also associated with the latent heat release. This warming increases the upward and downward emitted irradiance of clouds in those layers. For the lower layer, the absorption of the downward IR emitted from middle and upper clouds will also raise its temperature.

Overall, we suspect that multiple processes contribute to the increase in surface downward IR at Barrow. For the middle and upper layers, these processes include warm advection, water vapor advection, condensation with increases in cloudiness, and latent heat release, which all contribute to a greater downward IR at the surface. For the lower layer, the increase in the surface downward IR appears to arise mostly from warm advection.

We next address the question of whether other mechanisms, in addition to the TEAM mechanism, can account for the downward IR anomalies and Arctic warming examined here. We consider three possible mechanisms: 1) the dynamically driven polar warming mechanism (Cai 2005, 2006; Lu and Cai 2009, 2010; Deng et al. 2012; Park et al. 2012), 2) the moisture flux mechanism (Langen and Alexeev 2007), and 3) the sea

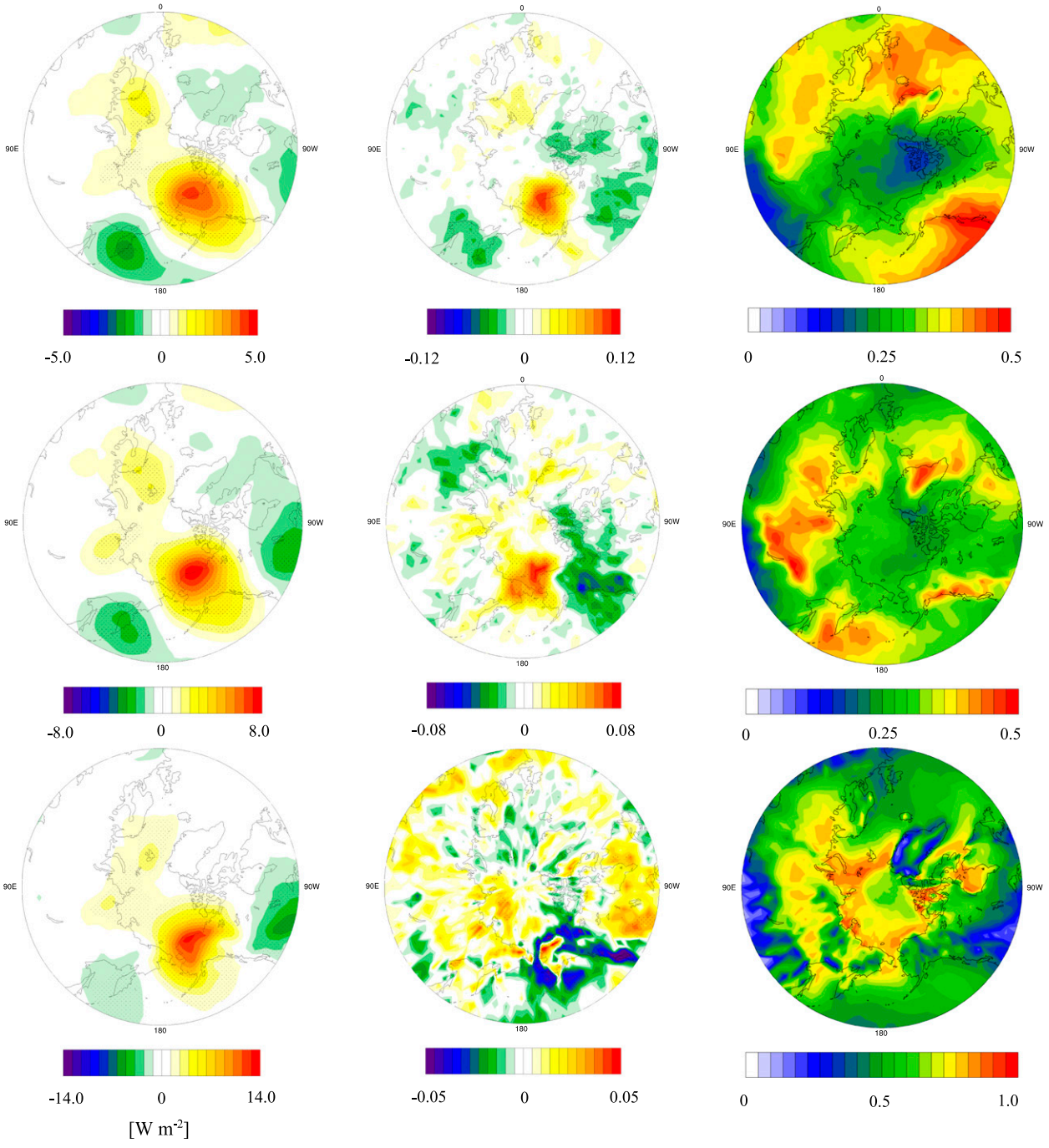

FIG. 9. Lagged regressions for lag 0 days of (left) σT^4 and (center) ERA-Interim cloud fraction against the BSRN Barrow downward IR, along with (right) the winter-mean cloud fraction over the 17-yr record for (top) the upper layer, (middle) the middle layer, and (bottom) the lower layer. Dots indicate statistical significance at the 95% confidence level.

ice albedo feedback mechanism (Stroeve et al. 2012). Since mechanisms 1 and 2 are based on steady-state solutions, these mechanisms may operate at intraseasonal and longer time scales. Mechanism 3, which operates on the seasonal time scale (heat stored during the warm season is released during the cold season), may take the form of episodic, intraseasonal evaporation events from the Arctic Ocean.

To evaluate whether the intraseasonal downward IR and surface warming fluctuations at Barrow analyzed in

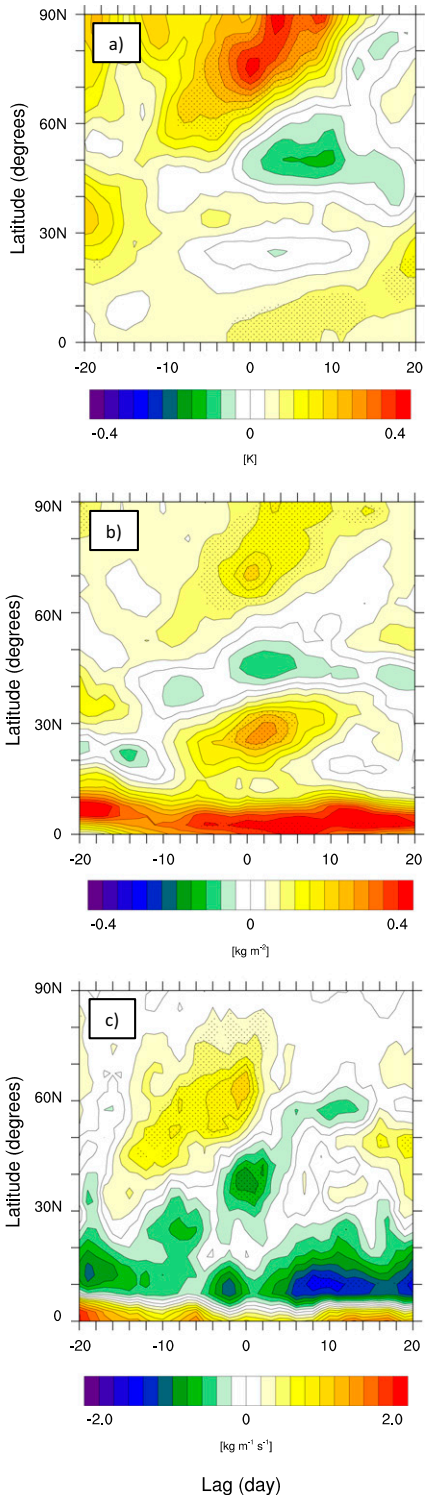

FIG. 10. Lagged regressions of the zonally averaged (a) 400-hPa temperature, (b) vertically integrated water vapor, and (c) vertically integrated northward water vapor flux against the Barrow downward IR as a function of latitude. Dots indicate statistical significance at the 95% confidence level.

this study are associated with the dynamically driven polar warming mechanism, we perform time-lagged regressions of the zonally averaged 400-hPa temperature against the Barrow downward IR (see Fig. 10a). The theory was developed to explain the increase in Arctic surface temperature in response to anthropogenic radiative forcing, and one crucial component of the theory is that an enhancement of the meridional temperature gradient in the upper troposphere leads to an increased poleward heat flux and a warmer Arctic. To test if this diffusive flux–gradient relationship operates in the Barrow downward IR events, we examine if the upper-tropospheric temperature gradient is enhanced prior to the maximum downward IR at Barrow. As can be seen, following the peak in tropical convection between lag −10 and lag −6 days, the meridional temperature gradient poleward of 40°N is anomalously weak for all subsequent lags. Equatorward of 15°N, where the convection takes place (Fig. 5), the anomalous meridional temperature gradient is close to zero from lag −10 to lag −3 days. That is, the increase in Barrow downward IR is not preceded by an increase in the upper-tropospheric meridional temperature gradient. The results are similar when regressing the Barrow downward IR against other upper-tropospheric temperature fields [e.g., at 450 and 500 hPa (not shown)]. The fact that the diffusive flux–gradient relationship is not involved in the Barrow downward IR and warming is consistent with the TEAM mechanism, where the poleward heat transport does not rely on the flux–gradient relationship and instead occurs through constructive interference between planetary-scale stationary and transient waves (Baggett and Lee 2015). This process, which can be described as arising from a forced tapping of the zonal available potential energy by Rossby waves excited by warm pool tropical convection, is independent of the equator-to-pole temperature gradient.

To examine whether the moisture flux mechanism contributes to the Barrow downward IR increases shown in this study, we regress the zonally averaged and vertically integrated water vapor and northward water vapor flux against the Barrow downward IR. If the downward IR at Barrow can be explained by this mechanism, we would expect the Barrow downward IR to be linked with an increase in the gradient of the vertically integrated water vapor over much of the Northern Hemisphere and an enhanced poleward water vapor flux that extends from the tropics to the Arctic. We do not find either of these signals in the regressed fields. Rather, near lag 0 days, we find large increases in water vapor at 30° and 70°N (approximately the latitude of Barrow) (Fig. 10b), as well as an anomalous equatorward water vapor flux (Fig. 10c) south of 50°N. These

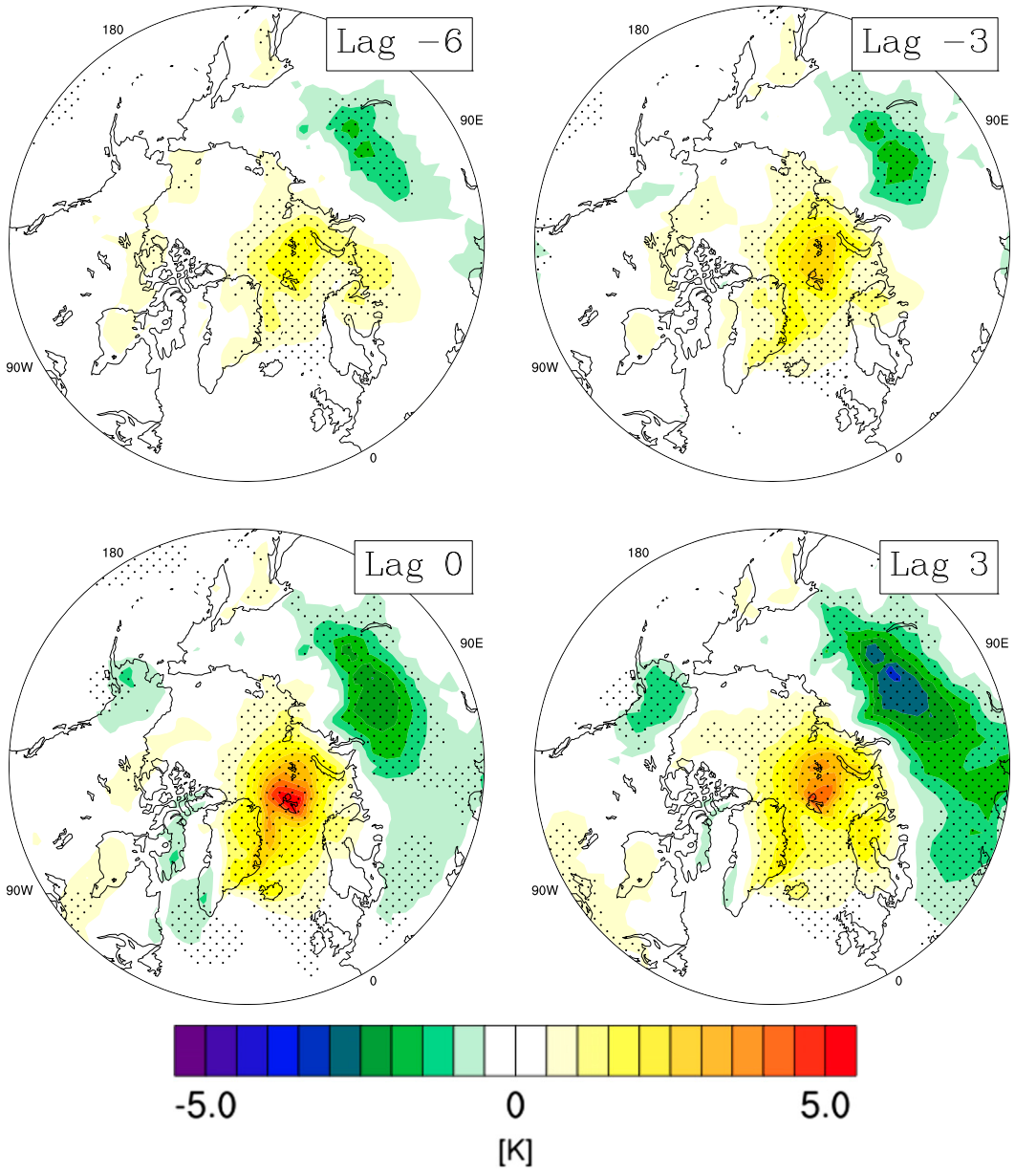

FIG. 11. As in Fig. 2, but for the BSRN Ny-Ålesund downward IR.

results suggest that this particular mechanism does not contribute to the increase in the Barrow downward IR found in this study. Furthermore, if the downward IR fluctuations at Barrow were influenced solely by water vapor fluxes, the enhanced emissivity due to the increased water vapor and cloudiness would lead to a decline in the upper-tropospheric temperature because of greater radiative cooling. However, the increase in the upper-tropospheric temperature (Fig. 10a) indicates otherwise, suggesting that poleward heat fluxes play an important role. In addition, the tilting of the largest 400-hPa temperature contours toward high latitudes with increasing lag is also consistent with heat fluxes contributing to the Arctic warming.

Last, to investigate the possible role of the sea ice albedo feedback mechanism, we compute time-lagged regressions of the surface evaporation against the Barrow downward IR (see the right column in Fig. 7). If the sea ice albedo feedback from the previous summer was influencing the intraseasonal downward IR fluctuations at Barrow, we would expect to see an increase in the surface evaporation over the Arctic Ocean near Barrow.

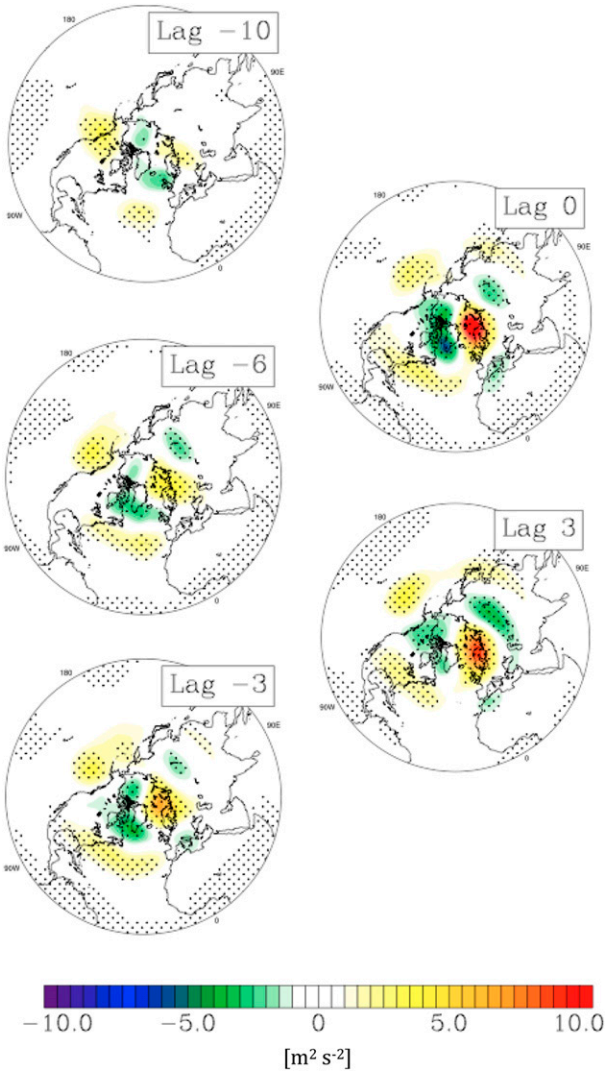

FIG. 12. As in Fig. 3, but for the BSRN Ny-Ålesund downward IR.

As can be seen, we find a strong connection between increasing downward IR at Barrow and surface evaporation (i.e., from the ocean surface to the atmosphere) from lag −2 to lag 0 days. However, these surface evaporation anomalies occur in the Bering Sea and Gulf of Alaska, far from Barrow, and well to the south of the September marginal sea ice zone (http://nsidc.org).

It is important to mention that the results shown in Fig. 10 do not invalidate the above three mechanisms. Rather, in the context of the intraseasonal downward IR and surface warming fluctuations at Barrow, we did not find evidence that these mechanisms are operating. In fact, it is plausible that these mechanisms may play an important role for other intraseasonal processes and for longer-time-scale processes.

b. Ny-Ålesund downward IR

As for Barrow, the regression of the 2-m temperature field against the Ny-Ålesund downward IR shows a maximum value at lag 0 days (Fig. 11), with temperature growth and decay time scales comparable to the downward IR *e*-folding time scale. Next, the link between the Ny-Ålesund downward IR and circulation at lower latitudes is examined by regressing the 300-hPa geopotential height field against the Ny-Ålesund downward IR (Fig. 12). As for Barrow, the Ny-Ålesund downward IR is also preceded by a statistically significant Rossby wave train, however this wave train is centered over the northwestern Atlantic, northern Canada, and Scandinavia (Fig. 12), with the latter two centers reaching their maximum amplitude at lag 0 days and decaying afterward. A weaker anomaly, which is also statistically significant, is present over the northeastern Pacific.

To investigate if this wave train is also associated with tropical convection, the tropical OLR is regressed against the Ny-Ålesund downward IR. Our results suggest a tropical influence from both oceans (see Fig. 13). At lag −15 days, one can see a large negative OLR anomaly in the Pacific warm pool and a large positive anomaly over the central tropical Pacific Ocean. These OLR anomalies generally appear to weaken with time but remain statistically significant. However, regressions of the Wheeler and Hendon (2004) MJO index (not shown) do not indicate a statistically significant link to the MJO. The northeastern Pacific 300-hPa geopotential height anomaly in Fig. 12 is closer to the positive OLR anomaly over the central tropical Pacific Ocean than to the negative anomaly over the Pacific warm pool, which suggests that the Pacific wave train may have central Pacific origins. However, the absence of a large geopotential height anomaly over the subtropical Pacific makes it difficult to determine with confidence the source region for this wave train. A large amplitude OLR anomaly that strengthens with time is also observed over the western tropical Atlantic Ocean. The presence of a positive 300-hPa geopotential height anomaly over the northwestern Atlantic that is located to the northwest of the negative tropical OLR anomaly is consistent with the North Atlantic wave train being driven by Atlantic tropical convection. As with Barrow, these findings suggest that tropical convection also contributes to the Ny-Ålesund Arctic downward IR anomaly.

To examine the possible linkage between the downward IR at Ny-Ålesund and moist processes, as for Barrow, we regress the ERA-Interim vertically integrated water vapor flux and water vapor flux convergence, cloud liquid and frozen water contents, and

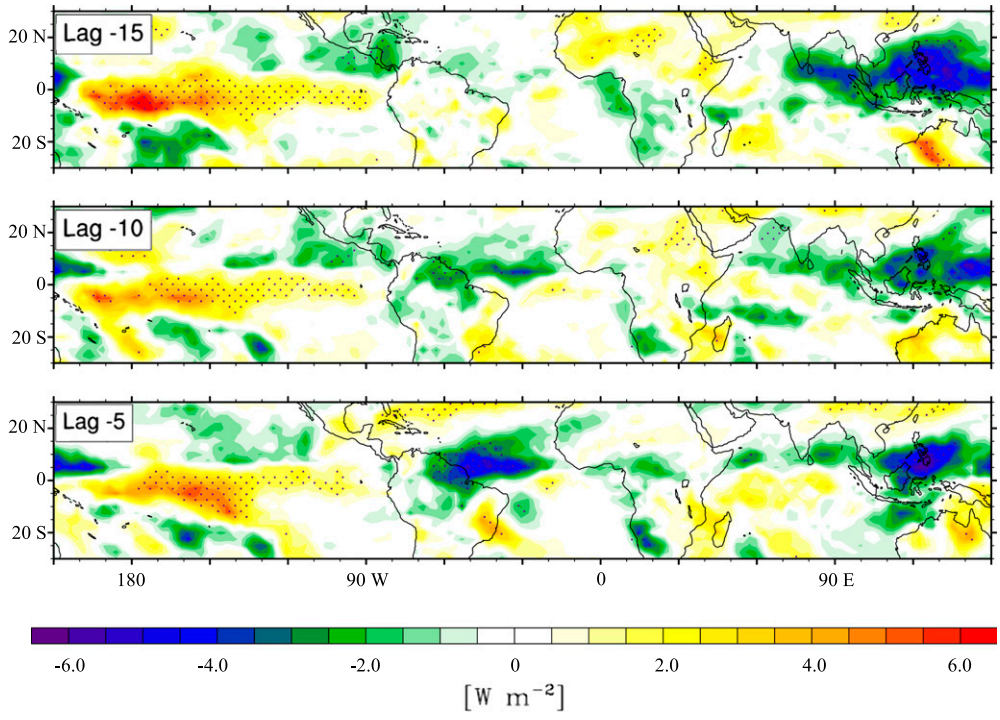

FIG. 13. As in Fig. 5, but for the BSRN Ny-Ålesund downward IR.

downward IR against the Ny-Ålesund downward IR. Similar to that in Barrow, the regressed vertically integrated water vapor flux (Fig. 14, left column) shows a large poleward flux of water vapor extending from the midlatitude North Atlantic toward Ny-Ålesund. This results in a region of water vapor flux convergence spanning the North Atlantic from eastern Greenland to Ny-Ålesund. Again, as for Barrow, there is an increase in both cloud liquid water (Fig. 14, center column, top panel) and cloud frozen water (Fig. 14, center column, bottom panel) by lag 0 days. However, regressions of cloud liquid water flux convergence were small and not statistically significant (not shown).

Regression of the ERA-Interim downward IR against the Ny-Ålesund downward IR (Fig. 14, right column) reveals a spatial pattern and amplitude closely resembling that of the water vapor flux convergence multiplied by the latent heat of vaporization, ultimately suggesting that the same processes driving changes in downward IR at Barrow are also operating at Ny-Ålesund.

Last, as with Barrow, attribution calculations were performed to examine whether the dynamically driven polar warming mechanism, the moisture flux mechanism, and the sea ice albedo feedback mechanism are related to the intraseasonal increases in downward IR at Ny-Ålesund. For the sake of brevity, the results are not shown. With regard to the former two mechanisms, our findings yield the same conclusions as with the Barrow downward IR. That is, lagged regressions against Ny-Ålesund downward IR find a reduced meridional gradient of the zonally averaged 400-hPa temperature, a reduction of the gradient of the zonally averaged and vertically integrated water vapor, and an equatorward vertically integrated water vapor flux south of 45°N. However, for the sea ice albedo feedback mechanism, positive, statistically significant surface evaporation anomalies beginning at lag −6 days suggest that this mechanism may contribute to the downward IR increase.

4. Summary and conclusions

This study examines the role of downward IR anomalies in driving the Arctic surface warming associated with the TEAM mechanism, which is hypothesized to influence polar amplification [Lee et al. (2011); Lee (2012); see the review by Lee (2014)]. In previous studies of the TEAM mechanism, it was shown that enhanced warm pool tropical convection excites poleward-propagating Rossby wave trains that are followed by Arctic surface warming due, in large part, to an increase in downward IR. However, since these studies relied solely on reanalysis downward IR

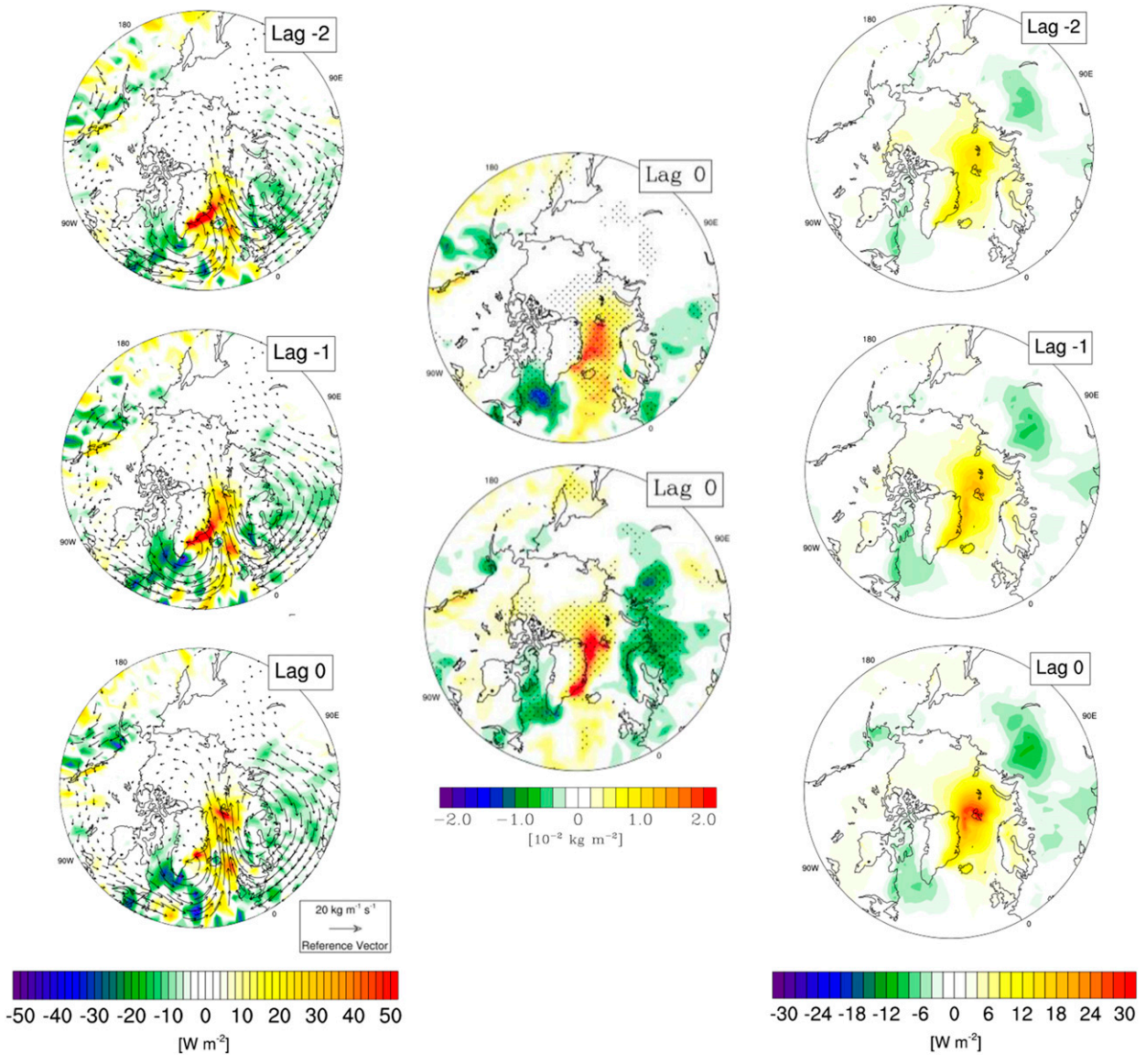

FIG. 14. Lagged regressions of (left) water vapor flux (vectors) and water vapor flux convergence multiplied by the latent heat of vaporization (shading), and (right) the ERA-Interim downward IR against the BSRN Ny-Ålesund downward IR. (center) The lag-0-day regression of the (top) cloud liquid water and (bottom) cloud frozen water against the BSRN Ny-Ålesund downward IR are also shown. Dots indicate statistical significance at the 95% confidence level.

data, which have an important modeling component, we use in situ downward IR data from two Arctic BSRN stations to further support the veracity of the TEAM mechanism.

By regressing key variables against downward IR at the Arctic BSRN stations, we found close agreement with past studies, in that changes in station downward IR are preceded by 1–2 weeks by anomalies in tropical convection and poleward Rossby wave propagation. For Barrow, an increase in downward IR is associated with increased (decreased) convection over the western tropical Pacific (Indian) Ocean, an active MJO, and a wave train that closely resembles the PNA teleconnection pattern. For Ny-Ålesund, the increase in downward IR is preceded by reduced (enhanced) convection over the central tropical Pacific (Indo–western Pacific warm pool), along with an increase in convection over the western tropical Atlantic. In this case, the tropical convection is not associated with the MJO, and the flow field is dominated by a wave train extending over eastern North America and the northwestern Atlantic. For both Barrow and Ny-Ålesund, the location of the wave trains

relative to the convection is consistent with the wave trains being excited by the convection.

We also used linear regressions to investigate the physical mechanisms that link the Rossby wave train and Arctic downward IR. It was found for both Barrow and Ny-Ålesund that the wave train advects heat and water vapor from midlatitudes into the Arctic. Since the resulting water vapor flux convergence multiplied by the latent heat of vaporization closely resembles the increase in downward IR both in spatial pattern and in amplitude, it appears that latent heat due to condensation (both cloud liquid and frozen water increase) contributed to an increase in atmospheric temperature followed by increased downward IR. Furthermore, it is found that warm advection throughout the troposphere and increased cloud cover in the upper and middle troposphere are also likely contributors to a larger downward IR. In addition, at Ny-Ålesund, enhanced surface evaporation anomalies suggest that the sea ice albedo feedback mechanism may contribute to increased downward IR at that location. Since ERA-Interim downward IR closely resembles the BSRN downward IR at Barrow and Ny-Ålesund, we speculate that surface warming over much of the Arctic is driven by the same processes. A full radiative transfer analysis with station data, which involves vertical profiles of cloudiness (both liquid and ice clouds), water vapor, temperature, and radiative variables during periods of large downward IR associated with the TEAM mechanism, is the focus of our next project.

Acknowledgments. This study is supported by National Science Foundation Grants AGS-1139970, AGS-1036858, and AGS-1401220 and National Oceanic and Atmospheric Administration Grant NA14OAR4310190. We thank two anonymous reviewers for their helpful comments. We also thank the European Centre for Medium-Range Weather Forecasts, the Climate Analysis Branch of the NOAA Earth System Research Laboratory/Physical Sciences Division, and the World Radiation Monitoring Center–Baseline Surface Radiation Network for making available the ERA-Interim data, the outgoing longwave radiation data, and the downward IR station data, respectively.

REFERENCES

Baggett, C., and S. Lee, 2015: Arctic warming induced by tropically forced tapping of available potential energy and the role of the planetary-scale waves. *J. Atmos. Sci.*, **72**, 1562–1568, doi:10.1175/JAS-D-14-0334.1.

Cai, M., 2005: Dynamical amplification of polar warming. *Geophys. Res. Lett.*, **32**, L22710, doi:10.1029/2005GL024481.

——, 2006: Dynamical greenhouse-plus feedback and polar warming amplification. Part I: A dry radiative-transportive climate model. *Climate Dyn.*, **26**, 661–675, doi:10.1007/s00382-005-0104-6.

Davis, R. E., 1976: Predictability of sea surface temperature and sea level pressure anomalies over the North Pacific Ocean. *J. Phys. Oceanogr.*, **6**, 249–266, doi:10.1175/1520-0485(1976)006<0249:POSSTA>2.0.CO;2.

Dee, D. P., and S. Uppala, 2009: Variational bias correction of satellite radiance data in the ERA-Interim reanalysis. *Quart. J. Roy. Meteor. Soc.*, **135**, 1830–1841, doi:10.1002/qj.493.

——, and Coauthors, 2011: The ERA-Interim reanalysis: Configuration and performance of the data assimilation system. *Quart. J. Roy. Meteor. Soc.*, **137**, 553–597, doi:10.1002/qj.828.

Deng, Y., T.-W. Park, and M. Cai, 2012: Process-based decomposition of the global surface temperature response to El Niño in boreal winter. *J. Atmos. Sci.*, **69**, 1706–1712, doi:10.1175/JAS-D-12-023.1.

Dutton, E. G., D. Halliwell, A. Herber, M. Maturilli, and V. Kustov, 2014: Basic measurements of radiation from the Baseline Surface Radiation Network (BSRN) of five stations in the years 1993 to 2013 for the December, January, and February seasons, reference list of 142 datasets. PANGEA, accessed 1 June 2012, doi:10.1594/PANGAEA.150003.

Feldstein, S. B., 2002: The recent trend and variance increase of the annular mode. *J. Climate*, **15**, 88–94, doi:10.1175/1520-0442(2002)015<0088:TRTAVI>2.0.CO;2.

Franzke, C., S. B. Feldstein, and S. Lee, 2011: Synoptic analysis of the Pacific–North American teleconnection pattern. *Quart. J. Roy. Meteor. Soc.*, **137**, 329–346, doi:10.1002/qj.768.

Hoskins, B. J., and D. J. Karoly, 1981: The steady linear response of a spherical atmosphere to thermal and orographic forcing. *J. Atmos. Sci.*, **38**, 1179–1196, doi:10.1175/1520-0469(1981)038<1179:TSLROA>2.0.CO;2.

——, M. E. McIntyre, and A. W. Robertson, 1985: On the use and significance of isentropic potential vorticity maps. *Quart. J. Roy. Meteor. Soc.*, **111**, 877–946, doi:10.1002/qj.49711147002.

Johnson, N. C., and S. B. Feldstein, 2010: The continuum of North Pacific sea level pressure patterns: Intraseasonal, interannual, and interdecadal variability. *J. Climate*, **23**, 851–867, doi:10.1175/2009JCLI3099.1.

Langen, P. L., and V. A. Alexeev, 2007: Polar amplification as a preferred response in an idealized aquaplanet GCM. *Climate Dyn.*, **29**, 305–317, doi:10.1007/s00382-006-0221-x.

Lee, S., 2012: Testing of the tropically excited Arctic warming mechanism (TEAM) with traditional El Niño and La Niña. *J. Climate*, **25**, 4015–4022, doi:10.1175/JCLI-D-12-00055.1.

——, 2014: A theory for polar amplification from a general circulation perspective. *Asia-Pac. J. Atmos. Sci.*, **50**, 31–43, doi:10.1007/s13143-014-0024-7.

——, T. Gong, N. Johnson, S. B. Feldstein, and D. Pollard, 2011: On the possible link between tropical convection and the Northern Hemisphere Arctic surface air temperature change between 1958 and 2001. *J. Climate*, **24**, 4350–4367, doi:10.1175/2011JCLI4003.1.

Lu, J., and M. Cai, 2009: Seasonality of polar surface warming amplification in climate simulations. *Geophys. Res. Lett.*, **36**, L16704, doi:10.1029/2009GL040133.

——, and ——, 2010: Quantifying contributions to polar warming amplification in an idealized coupled general circulation model. *Climate Dyn.*, **34**, 669–687, doi:10.1007/s00382-009-0673-x.

Maturilli, M., A. Herber, and G. König-Langlo, 2014: Surface radiation climatology for Ny-Ålesund, Svalbard (78.9°N), basic observations for trend detection. *Theor. Appl. Climatol.*, **120**, 331–339, doi:10.1007/s00704-014-1173-4.

Moore, R. W., O. Martius, and T. Spengler, 2010: The modulation of the subtropical and extratropical atmosphere in the Pacific basin in response to the Madden–Julian oscillation. *Mon. Wea. Rev.*, **138**, 2761–2779, doi:10.1175/2010MWR3194.1.

Mori, M., and M. Watanabe, 2008: The growth and triggering mechanisms of the PNA: A MJO–PNA coherence. *J. Meteor. Soc. Japan*, **86**, 213–236, doi:10.2151/jmsj.86.213.

Park, T.-W., Y. Deng, and M. Cai, 2012: Feedback attribution of the El Niño–Southern Oscillation-related atmospheric and surface temperature anomalies. *J. Geophys. Res.*, **117**, D23101, doi:10.1029/2012JD018468.

Roundy, P. E., K. MacRitchie, J. Asuma, and T. Melino, 2010: Modulation of the global atmospheric circulation by combined activity in the Madden–Julian oscillation and the El Niño–Southern Oscillation during boreal winter. *J. Climate*, **23**, 4045–4059, doi:10.1175/2010JCLI3446.1.

Stroeve, J. C., M. C. Serreze, M. M. Holland, J. E. Kay, J. Malanik, and A. P. Barrett, 2012: The Arctic's rapidly shrinking sea ice cover: A research synthesis. *Climate Change*, **110**, 1005–1027, doi:10.1007/s10584-011-0101-1.

Wheeler, M. C., and H. H. Hendon, 2004: An all-season real-time multivariate MJO index: Development of an index for monitoring and prediction. *Mon. Wea. Rev.*, **132**, 1917–1932, doi:10.1175/1520-0493(2004)132<1917:AARMMI>2.0.CO;2.

Yoo, C., S. Feldstein, and S. Lee, 2011: The impact of the Madden–Julian Oscillation trend on the Arctic amplification of surface air temperature during the 1979–2008 boreal winter. *Geophys. Res. Lett.*, **38**, L24804, doi:10.1029/2011GL049881.

——, S. Lee, and S. B. Feldstein, 2012a: Arctic response to an MJO-like tropical heating in an idealized GCM. *J. Atmos. Sci.*, **69**, 2379–2393, doi:10.1175/JAS-D-11-0261.1.

——, ——, and ——, 2012b: Mechanisms of Arctic surface air temperature change in response to the Madden–Julian oscillation. *J. Climate*, **25**, 5777–5790, doi:10.1175/JCLI-D-11-00566.1.

Zib, B. J., X. Dong, B. Xi, and A. Kennedy, 2012: Evaluation and intercomparison of cloud fraction and radiative fluxes in recent reanalyses over the Arctic using BSRN surface observations. *J. Climate*, **25**, 2291–2305, doi:10.1175/JCLI-D-11-00147.1.